Voltage Control of Rare-Earth Magnetic Moments at the Magnetic-Insulator–Metal Interface

Alejandro O. Leon,[1] Adam B. Cahaya,[1] and Gerrit E. W. Bauer[1,2]
[1]Institute for Materials Research, WPI-AIMR, and CSRN, Tohoku University, Sendai 980-8577, Japan
[2]Zernike Institute for Advanced Materials, University of Groningen, 9747 AG Groningen, The Netherlands

(Received 5 September 2017; published 10 January 2018)

The large spin-orbit interaction in the lanthanides implies a strong coupling between their internal charge and spin degrees of freedom. We formulate the coupling between the voltage and the local magnetic moments of rare-earth atoms with a partially filled $4f$ shell at the interface between an insulator and a metal. The rare-earth-mediated torques allow the power-efficient control of spintronic devices by electric-field-induced ferromagnetic resonance and magnetization switching.

DOI: 10.1103/PhysRevLett.120.027201

Introduction.—The power demand for magnetization control in magnetic memories is an important design parameter. The power consumption of voltage-driven magnetization dynamics can be orders of magnitude lower than the one of electric-current-induced dynamics [1]. In addition, electric voltages are a more localized driving mechanism compared to magnetic fields [1]. From the experimental point of view, magnetization reversal [2,3] and ferromagnetic resonance [1,4] driven by electric voltages have been achieved. In those studies, transition-metal films are capped with an insulating barrier that prevents the electric current flow. The main mechanism to couple voltage and magnetization is the control of the perpendicular magnetic anisotropy [5]. The magnetization has been manipulated by electric fields for the first time in (Ga,Mn)As [6] and also in magnetoelectric materials [7–9].

The spin-charge coupling that causes the observed phenomena has been modeled by the Rashba [10,11] and Dzyaloshinskii-Moriya interactions [11–13], whose origin is the relativistic magnetic field induced by *linear momentum* of the electron in a transverse electric field. On the other hand, the spin-orbit interaction in central fields of single atoms can best be expressed in terms of the effective magnetic field generated by orbital *angular momentum*. Here we focus on local magnetic moments in a condensed matter system for which the second picture of the spin-orbit interaction is the best starting point.

Local magnetic moments in solids are formed by partially filled $3d$ and $4f$ shells of transition metals and rare earths, respectively. The former are relatively light, and their spin dynamics are dominated by the exchange interaction, with correction by the crystal fields. Rare earths (REs), on the other hand, have their magnetic subshell shielded by outer shells, which decreases the effect of crystal fields and allows the electrons to orbit almost freely in the central Coulomb field of the ionic core with large nuclear charges. The spin-orbit interaction (SOI) of REs is therefore large and free-atomic-like. Since SOI couples the electric and magnetic degrees of freedom, we may expect significant effects of electric fields on the RE magnetization dynamics. Control and switching of RE moments by crystal fields in multiferroic systems has been predicted [14].

Here we study the voltage-driven dynamics of rare earths at the interface between a magnetic insulator (or bad conductor) and a metal. When one of the layers is magnetic, the presence of REs at the interface strongly couples the magnetization to an applied static and dynamic voltage by the local spin-orbit interaction. Electric fields, applied by high-frequency signal generators, for example, are constant inside an insulator but nearly vanish in a metal. The large spatial gradients of the electric field at the interface renormalize the RE electrostatic interactions with neighboring atoms (crystal fields) and appear as a voltage-modulated magnetic anisotropy and the associated magnetization torque that we derive in the following in more detail.

Magnetism of rare-earth ions.—In the Russell-Saunders scheme [15], the total spin ($\mathbf{S}$) and orbital ($\mathbf{L}$) momenta are the sum of the single-electron momenta of the $4f$ orbitals $\mathbf{S}=\sum_j \mathbf{s}_j$ and $\mathbf{L}=\sum_j \mathbf{l}_j$. The spin-orbit coupling reads $H_{\mathrm{SOI}}=\Lambda \mathbf{S}\cdot\mathbf{L}$, and the coupling parameter Λ is positive (negative) for less (more) than a half filled subshell [15,16]. The total angular momentum vector $\mathbf{J}=\mathbf{S}+\mathbf{L}$ and the angular part of the eigenfunctions can be written as $|\Psi\rangle = |S,L,J,J_z\rangle$, where the quantum numbers are governed by $\mathbf{S}^2|\Psi\rangle=\hbar^2 S(S+1)|\Psi\rangle$, $\mathbf{L}^2|\Psi\rangle=\hbar^2 L(L+1)|\Psi\rangle$, $\mathbf{J}^2|\Psi\rangle=\hbar^2 J(J+1)|\Psi\rangle$, and $\hat{J}_z|\Psi\rangle=\hbar J_z|\Psi\rangle$, $\hat{J}_z$ is the z component of the vector $\mathbf{J}$, and $\hbar$ is Planck's constant divided by 2π. The lowest-energy state of RE ions as governed by Hund's rules [15] are listed in Table I. The Wigner-Eckart theorem ensures that within this ground state manifold the angular momenta are collinear, viz. $\mathbf{S}=(g_J-1)\mathbf{J}$ and $\mathbf{L}=(2-g_J)\mathbf{J}$ in terms of the Landé g factor g_J. Furthermore, for constant (S,L,J), the orbital symmetry axis and the spin vector move rigidly together [17,18], implying that the atomic charge and spin distributions are strongly locked by the spin-orbit

TABLE I. Ground state (S, L, J) based on Hund's rules and shape of the $4f$ ground state electron density [17]. Q_2 is the quadrupole moment calculated using the Wigner-Eckart theorem for the state $J_z = J$, and $a_0 = 0.53$ Å is the Bohr radius. The Wigner-Eckart theorem cannot be applied to Eu because $\mathbf{J} = 0$.

Ion	$4f^n$	S	L	J	Shape	Q_2/a_0^2
Ce^{3+}	$4f^1$	$\frac{1}{2}$	3	$\frac{5}{2}$	Oblate	−0.686
Pr^{3+}	$4f^2$	1	5	4	Oblate	−0.639
Nd^{3+}	$4f^3$	$\frac{3}{2}$	6	$\frac{9}{2}$	Oblate	−0.232
Pm^{3+}	$4f^4$	2	6	4	Prolate	0.202
Sm^{3+}	$4f^5$	$\frac{5}{2}$	5	$\frac{5}{2}$	Prolate	0.364
Eu^{3+}	$4f^6$	3	3	0	...	...
Gd^{3+}	$4f^7$	$\frac{7}{2}$	0	$\frac{7}{2}$	Spherical	0
Tb^{3+}	$4f^8$	3	3	6	Oblate	−0.505
Dy^{3+}	$4f^9$	$\frac{5}{2}$	5	$\frac{15}{2}$	Oblate	−0.484
Ho^{3+}	$4f^{10}$	2	6	8	Oblate	−0.185
Er^{3+}	$4f^{11}$	$\frac{3}{2}$	6	$\frac{15}{2}$	Prolate	0.178
Tm^{3+}	$4f^{12}$	1	5	6	Prolate	0.427
Yb^{3+}	$4f^{13}$	$\frac{1}{2}$	3	$\frac{7}{2}$	Prolate	0.409

interaction. The electron density of a partially filled $4f$ subshell can be written as

$$n_{4f}(\mathbf{r}) = \sum_{m_l=-3}^{3} |R_{4f}(r) Y_3^{m_l}(\hat{\mathbf{r}})|^2 (f_{m_l\uparrow} + f_{m_l\downarrow}), \quad (1)$$

where $\mathbf{r} = r\hat{\mathbf{r}}$ is the position vector in spherical coordinates, $R_{4f}(r)$ is (approximately) the radial part of the $4f$ atomiclike wave function, and the spherical harmonic $Y_3^{m_l}(\hat{\mathbf{r}})$ describe the angular dependence. f_{m_l,m_s} is the occupation number of the single-electron state with magnetic quantum numbers of orbital m_l and spin m_s angular momenta. The density n_{4f} is normalized to the number of electrons in the $4f$ shell $N_{4f} = \int n_{4f}(\mathbf{r}, t) d\mathbf{r}$. The typical $4f$ radius $\langle r \rangle \sim 0.5$ Å is much smaller than typical interatomic distances $R \sim 3$ Å, which motivates the multipole expansion [17,18]

$$n_{4f}(\mathbf{r}) \approx \frac{|R_{4f}(r)|^2}{4\pi} \left(N_{4f} + \frac{5Q_2}{4\langle r^2 \rangle} [3(\mathbf{m} \cdot \hat{\mathbf{r}})^2 - 1] \right), \quad (2)$$

where $Q_2 \equiv \int (3z^2 - r^2) n_{4f}(\mathbf{r}) d\mathbf{r}$ is the quadrupole moment listed in Table I. $\mathbf{m} = -\mathbf{J}/|\mathbf{J}|$ is the unit magnetization vector that at equilibrium is taken to be $\mathbf{e}_z$ but in an excited state may depend on time. The unit position vector in spherical coordinates is $\hat{\mathbf{r}} = \sin\theta[\mathbf{e}_x \cos\phi + \mathbf{e}_y \sin\phi] + \mathbf{e}_z \cos\theta$, where $\{\mathbf{e}_x, \mathbf{e}_y, \mathbf{e}_z\}$ are the unit vectors along the Cartesian axes. For $Q_2 > 0$ ($Q_2 < 0$), the envelope function of the electron density is a pancake or cigarlike (oblate or prolate) ellipsoid, respectively.

A local magnetic ion interacts weakly with static electric fields, $\mathbf{E} = -\nabla V$, where V is the voltage or potential energy of a positive probe charge. To leading order, the ions experience the electrostatic energy [19]

$$\langle \psi | - e \sum_{i=1}^{N_{4f}} V(\mathbf{r}_i) | \psi \rangle = -e \int d^3 r V(\mathbf{r}) n_{4f}(\mathbf{r}), \quad (3)$$

where $-e$ is the electron charge and $-eV(\mathbf{r}_i)$ is the potential energy of the ith electron. $|\psi\rangle$ is the $4f$ many-electron wave function in the ground state. Again, the leading order in a multipole expansion of the crystal field around the origin $r = 0$ can be parameterized by a quadrupolar term $A_2^{(0)}$:

$$eV(\mathbf{r}) = -A_2^{(0)} r^2 (3\cos^2\theta - 1). \quad (4)$$

Inserting Eqs. (2) and (4) into Eq. (3), we arrive at a Hamiltonian that depends on the magnetization direction as

$$H_{\text{ani}} = \frac{3}{2} Q_2 A_2^{(0)} m_z^2. \quad (5)$$

The crystal symmetry orients here the easy ($Q_2 A_2^{(0)} < 0$) or hard ($Q_2 A_2^{(0)} > 0$) magnetic axis along the z direction. This *crystal field* energy accounts for the single rare-earth ion magnetic anisotropy. The parameter $A_0^{(2)}$ can be calculated by first principles or to fit to experiments. Typical values are $A_0^{(2)} = 300$ Ka_0^{-2} for $(\text{RE})_2\text{Fe}_{14}\text{B}$, $A_0^{(2)} = 34$ Ka_0^{-2} for $(\text{RE})_2\text{Fe}_{17}$, and $A_0^{(2)} = -358$ Ka_0^{-2} for $(\text{RE})_2\text{Fe}_{17}\text{N}_3$ [18], where $a_0 = 0.53$ Å is the Bohr radius. The origin of the strong magnetic anisotropy of REs is their large spin-orbit interactions. On the other hand, for $3d$ transition-metal moments, the anisotropy is usually very small, except at interfaces, where the orbital motions are partially unquenched. In such cases, the anisotropy emerges as the consequence of SOI, the quadrupolar shape of electric potentials at the interface [5], the hybridization of orbitals, and change in the orbital occupation.

At an interface between materials with different work functions, the symmetry is reduced. The electric field exhibits spatial gradients due to charge accumulation immediately at the interface that result in a step like potential. An external voltage difference ΔV drops over the insulator but is constant in the metal (when the ferromagnet is a bad conductor, the effects are weaker but still exist). The electric field field gradient couples to quadrupoles in the immediate proximity of the interface.

Voltage coupling at interfaces.—Let us focus on a magnetic-insulator film with thickness L_F. At the surface, the insulator exposes n_{RE} rare-earth moments per unit of area. Inside the insulator, the electric field is approximately constant, $\mathbf{E}(z < 0) = \mathbf{e}_z \Delta V / L_F$, while it vanishes in the metal $\mathbf{E}(z > 0) = 0$; see Fig. 1(a). Using Eq. (3), the electric energy of a magnetic moment at the origin is then

$$H_e = H_0 - \frac{15}{64} \frac{e\Delta V}{L_F} Q_2 \frac{\langle r \rangle}{\langle r^2 \rangle} m_z^2, \quad (6)$$

where $H_0 = 5eE_0 Q_2 \langle r \rangle / (64\langle r^2 \rangle) + e(\Delta V / L_F) N_{4f} \langle r \rangle / 4$ does not depend on the magnetization and $\langle r^n \rangle \equiv N_{4f}^{-1} \int r^n n_{4f}(\mathbf{r}) d\mathbf{r}$. For $\langle r^2 \rangle^{1/2} \sim \langle r \rangle \sim 0.5$ Å the coupling energy per unit area at equilibrium ($m_z^2 = 1$),

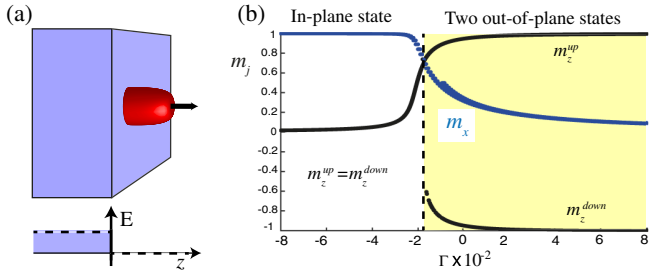

FIG. 1. Spin-charge coupling for an interface local magnetic moment. (a) Electric field at an interface between an insulator (constant electric field) and a metal (vanishing electric field). The magnetic dipole and charge quadrupole at the interface are coupled. (b) Ground state magnetization directions $\mathbf{m} = (m_x, m_y, m_z)$ as a function of the interface electric field with coupling parameter Γ [Eq. (9)] and a magnetic field tilted from the z axis by an angle $\varphi \sim 6°$. The system switches from a perpendicular easy-axis to an easy-plane configuration at $\Gamma < 0.018$.

$$\left| n_{\mathrm{RE}}(H_e - H_0)\frac{L_F}{\Delta V}\right| = 750\ \frac{\mathrm{fJ}}{\mathrm{V\,m}}\frac{Q_2}{10^{-3}\ \mathrm{nm}^2}\frac{n_{\mathrm{RE}}}{\mathrm{nm}^{-2}}, \quad (7)$$

is one order of magnitude larger than the corresponding coupling in transition metals [20,21]. For electric fields $\Delta V/L_F \sim 10\ \mathrm{mV/nm} = 100\ \mathrm{kV/cm}$, the surface energy density becomes $(H_e - H_0)n_{\mathrm{RE}} \approx 7.5 \times 10^{-3}\ \mathrm{erg/cm^2} = 7.5\ \mu\mathrm{J/m^2}$.

Our electrostatic model requires that the atomic terms of the $4f$ shell in the ground state are stable under applied electric fields, which possibly excludes valence fluctuation compounds. In the Supplemental Material [22] we show that a finite screening length leads to expressions very similar to Eq. (6). In good metals, exchange correlation modifies the screening only slightly and can therefore be disregarded here.

The step field model can also be applied to *nonmagnetic insulators* and *transition-metal ferromagnets* (such as Fe, Co, and Ni, or their alloys) with RE ions at the interface that are antiferromagnetically coupled to the magnetic order [25,26] and facilitate a large coupling of the magnetization to electric fields. Good insulators, such as MgO, can endure very large electric fields (of the order of 300 mV/nm, in FeCo|MgO, Ref. [20], for example). Thus, MgO-based magnetic tunnel junctions with rare-earth doping or dusting are promising devices to study and apply electric-field-induced modulations of the magnetization configuration.

In magnetic materials, local angular momenta are strongly locked by the exchange interaction. When a sufficiently strong static magnetic field $\mathbf{B}$ is applied, the macrospin model is valid; i.e., the magnetization $\mathbf{M}$ is constant in space. The total magnetic energy H_M per unit area then reads

$$\frac{H_M}{\mu_0 M_s^2 L_F} = -\mathbf{m}\cdot\mathbf{h} - \frac{\beta_x}{2}m_x^2 + \frac{\beta_z - \Gamma}{2}m_z^2. \quad (8)$$

The first term on the (dimensionless) right-hand side with $\mathbf{h} = \mathbf{B}/(\mu_0 M_s)$ is the Zeeman energy and M_s the saturation magnetization. The parameters β_x (β_z) account for the in-plane (out-of-plane) magnetic anisotropy in the absence of applied electric fields, $\Delta V = 0$. The dimensionless coupling parameter Γ measures the relative strength of the electrostatic coupling $\sim n_{\mathrm{RE}} e \Delta V Q_2/L_F$ that should be compared with magnetic anisotropies. $\Gamma \sim 0.06$ with the following parameters representative for a rare-earth iron garnet thin film such as $Tm_3Fe_5O_{12}$:

$$\Gamma = 0.06\frac{n_{\mathrm{RE}}}{1/\mathrm{nm}^2}\left(\frac{10^5\ \mathrm{A/m}}{M_s}\right)^2\left(\frac{10\ \mathrm{nm}}{L_F}\right)^2\frac{\Delta V}{0.1\ \mathrm{V}}\frac{Q_2}{10^{-3}\ \mathrm{nm}^2}. \quad (9)$$

Since the M_s of 8-nm-thick $Tm_3Fe_5O_{12}$ [27] is at room temperature about 10 times smaller than that of even a subnanometer FeCo film [20], the coupling strength Γ is 10 times larger for magnetic insulators for the same applied electric field without the need for additional tunnel barriers. Intraband transition and electric breakdown is of no concern as long as $eE_0 \ll \epsilon_{\mathrm{gap}}^2/(\epsilon_F a)$, where ϵ_{gap} is the band gap, ϵ_F the Fermi level in the metal, and a the lattice constant [28]. Using $\epsilon_F \sim 2$ eV, and the gap or lattice constant for yttrium iron garnet (YIG) [29,30] $\epsilon_{\mathrm{gap}} \sim 2.85\ \mathrm{eV}/a = 1.2$ nm, we estimate $E_0 \ll 2\ \mathrm{V/nm}$ to be safe. The coupling strength Γ decreases $\sim L_F^{-2}$ for a given voltage, so much can be gained by choosing an insulator with a large gap and breakdown voltage that permits working with thin layers.

Figure 1(b) shows the stable magnetizations that minimize of the energy (8) in the presence of a magnetic field $\mathbf{h} = h[\mathbf{e}_x \cos\varphi + \mathbf{e}_z \sin\varphi]$ that is tilted by an angle φ. The parameter are $h = 0.01$, $\varphi = 5.72°$, $\beta_x = 0$, and $\beta_z = -0.03$. The application of a constant voltage allows the transition from the easy-axis (right zone) to the easy-plane (left zone) configuration.

The electric field effects in transition-metal devices, as well as the one proposed here, derive from the same type of magnetic anisotropy, although the microscopic coupling mechanism is different. The phenomenology of electric-field-induced precessional dynamics as observed in transition-metal systems [31] does not differ from the one we expect for RE systems. The advantage of interface REs is the lower power consumption and the possibility of using a wider range of materials including magnetic insulators, such as YIG. The magnetization dynamics is described by the Landau-Lifshitz-Gilbert equation

$$\dot{\mathbf{m}} = -\gamma\mathbf{m}\times\mathbf{h}_{\mathrm{eff}} + \alpha\mathbf{m}\times\dot{\mathbf{m}}, \quad (10)$$

where α is the Gilbert damping constant, $\gamma > 0$ is the (modulus of the) gyromagnetic ratio, $\dot{\mathbf{m}}$ is the temporal derivative of $\mathbf{m}$, and the effective magnetic field $\mathbf{h}_{\mathrm{eff}}$ satisfies

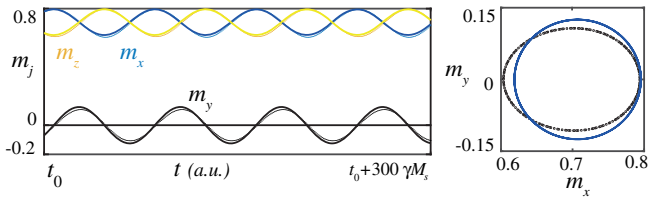

FIG. 2. (a) Magnetization dynamics induced by time-varying voltages. Comparison between analytic (solid line) and (b) numeric (dot) precessional (FMR) solutions, obtained for $\Gamma = \Gamma_0 \cos(\Omega t)$, $\Gamma_0 = 0.01$, $\beta_x = \beta_z = 0$, $\Omega = 0.08$, $h = 0.1$, $\varphi = 45°$, and $\alpha = 0.005$.

$$\frac{\mathbf{h}_{\rm eff}}{\mu_0 M_s} \equiv \frac{1}{\mu_0 M_s^2 L_F}\frac{\partial H_M}{\partial \mathbf{m}} = \mathbf{h} + \beta_x m_x \mathbf{e}_x + [\Gamma - \beta_z] m_z \mathbf{e}_z. \quad (11)$$

The magnetic torque exerted by the electric field is proportional to $-\mathbf{m} \times \gamma m_z \mathbf{e}_z$.

Ferromagnetic resonance.—We now turn to an ac electric field that modulates the coupling $\Gamma = \Gamma_0 \cos(\Omega t)$, with frequency Ω close to the ferromagnetic resonance (GHz). Since the electric field is normal to thin metallic films <100 nm, the induced Oersted-like magnetic field and associated power are negligibly small. In linear response, the model (10) can be solved analytically for $\beta_x = \beta_z = 0$. The polar coordinate system is spanned by the unit vectors $\mathbf{e}_1 = \mathbf{e}_x \cos\varphi + \mathbf{e}_z \sin\varphi$, $\mathbf{e}_2 = -\mathbf{e}_x \sin\varphi + \mathbf{e}_z \cos\varphi$, and $\mathbf{e}_3 = -\mathbf{e}_y$. At the equilibrium state, $\mathbf{m}_{\rm eq} = \mathbf{e}_1$ along the applied magnetic field. Around the equilibrium state, the magnetization is $\mathbf{m} = \mathbf{e}_1 + \delta\mathbf{m}$, where $\delta\mathbf{m} = \delta m_2 \mathbf{e}_2 + \delta m_3 \mathbf{e}_3$ is the deviation from $\mathbf{m}_{\rm eq}$, with $|\delta\mathbf{m}| \ll 1$ and $\delta\mathbf{m} \cdot \mathbf{m}_{\rm eq} = 0$. To leading order in the coupling (Γ_0) and dissipation (α), the effective field is $(\mu_0 M_s)^{-1}\mathbf{h}_{\rm eff} = h\mathbf{e}_1 + \Gamma \cos(\Omega t) \sin\varphi [\mathbf{e}_1 \sin\varphi + \mathbf{e}_2 \cos\varphi]$ and

$$\frac{\delta\dot{\mathbf{m}}}{\omega_M} = \mathbf{e}_1 \times \left[h\delta\mathbf{m} + \alpha\frac{\delta\dot{\mathbf{m}}}{\omega_M} - \frac{\Gamma_0}{2}\cos(\Omega t)\sin(2\varphi)\mathbf{e}_2 \right],$$

where $\omega_M \equiv \gamma\mu_0 M_s$. The effective ac magnetic field $\mathbf{B}_{\rm ac} = \mu_0 M_s \Gamma_0 \sin(2\varphi)\cos(\Omega t)\mathbf{e}_z/2$. Then

$$\begin{aligned}\delta\mathbf{m} = {} & (\Gamma_0/4)\sin(2\varphi)\chi'(\Omega)[\cos(\Omega t)\mathbf{e}_2 + \sin(\Omega t)\mathbf{e}_3] \\ & + (\Gamma_0/4)\sin(2\varphi)\chi''(\Omega)[\sin(\Omega t)\mathbf{e}_2 - \cos(\Omega t)\mathbf{e}_3],\end{aligned}$$

where χ' and χ'' are the real and imaginary parts, respectively, of the dynamics susceptibility

$$\chi(\omega) \equiv \frac{\omega_M(\omega_0 - \omega)}{(\omega_0 - \omega)^2 + \omega^2\alpha^2} + i\frac{\omega_M \alpha\omega}{(\omega_0 - \omega)^2 + \omega^2\alpha^2}$$

and the natural frequency is $\omega_0 \equiv \omega_M h = \gamma\mu_0 M_s h$. Figure 2 illustrates $\delta\mathbf{m}(t)$ (continuous lines) together with the numeric solution (dots). We see that a large oscillation cone $|\delta\mathbf{m}| \sim 0.15$ can be achieved by a relatively low voltage for the aforementioned parameter values and $\Gamma_0 = 0.01$ (or $\Delta V/L_F \sim 1.6$ mV/nm).

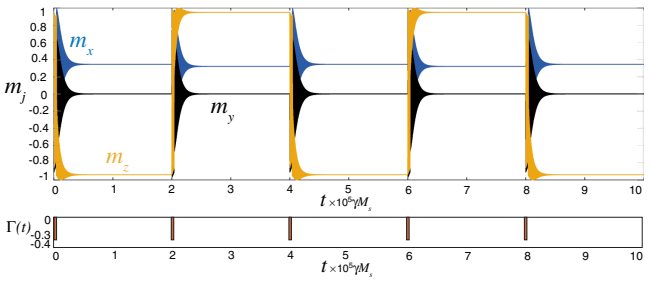

FIG. 3. Precessional switching for an easy-axis perpendicular magnet ($\beta_z = -0.03$) induced by a voltage box train. The upper panel shows the magnetization components, while the lower panel shows the box consisting of a negative voltage with $\Gamma = -0.03$ for $\Delta t = 4000\gamma M_s$ (~1 ns) followed by $\Gamma = 0$. This signal is repeated all $2 \times 10^5 \gamma M_s$ (~25 ns). Other parameters are $\beta_x = 0$, $h = 0.01$, $\varphi = 5.72°$, and $\alpha = 0.005$.

Magnetization switching.—Magnetic reversal in tunnel junctions is the key process in magnetic random access memories. An applied voltage can reduce the energy barrier for magnetic-field- and current-induced switching or directly trigger the magnetization reversal [31]. The latter effect is illustrated by Fig. 3 assuming perpendicular magnetization (for in-plane magnetization, see Refs. [2,3]). An equilibrium magnetization along z [either an *up* or *down* state in the right zone in Fig. 1(b)] is excited by a steplike voltage pulse into large damped precessions around the in-plane equilibrium [left zone in Fig. 1(b)]. When the voltage is turned off again at the right time, the magnetization can be fully reverted. The switching is observed with a large tolerance in the pulse duration between the pico- and nanosecond scales. In the simulation in Fig. 3, the pulse duration is around 1 ns, while the application of subsequent pulses toggles the magnetization direction faithfully.

Conclusions and remarks.—We report voltage-modulated magnetic anisotropies and magnetization dynamics of rare-earth magnetic moments at insulator-metal bilayer interfaces. An applied voltage generates inhomogeneous electric fields at interfaces with a large conductivity mismatch that couple efficiently to rare-earth ions with nonspherical electron distributions, i.e., when the shell is not half or completely filled. The voltage can then rigidly precess the charge and spin distributions of the entire $4f$ subshell via a stronger and direct coupling to the spin than in transition metals. The localized character of $4f$ electrons allow us to derive the leading order voltage coupling using *single-ion-like* and step field models without having to carry out first-principles calculations (that are essential for transition-metal systems). Adding rare-earth impurities to insulator-metal bilayers can be used to efficiently switch the magnetization and induce ferromagnetic resonance. Future applications may include rare-earth-dusted magnetic-insulator–normal-metal interfaces, such as YIG|Pt, that

can efficiently convert an ac voltage into a spin current by spin pumping.

We acknowledge the financial support from JSPS KAKENHI Grants No. 25247056, No. 25220910, and No. 26103006, JSPS Fellowship for Young Scientists No. JP15J02585, and CONICYT Becas Chile No. 74170017. We thank J. Barker for useful discussions. We profited from preparatory research by Dr. Mojtaba Rahimi.

[1] T. Nozaki, Y. Shiota, S. Miwa, S. Murakami, F. Bonell, S. Ishibashi, H. Kubota, K. Yakushiji, T. Saruya, A. Fukushima, S. Yuasa, T. Shinjo, and Y. Suzuki, Electric-field-induced ferromagnetic resonance excitation in an ultrathin ferromagnetic metal layer, Nat. Phys. **8**, 491 (2012).

[2] Y. Shiota, T. Maruyama, T. Nozaki, T. Shinjo, M. Shiraishi, and Y. Suzuki, Voltage-assisted magnetization switching in ultrathin $Fe_{80}Co_{20}$ alloy layers, Appl. Phys. Express **2**, 063001 (2009).

[3] S. Kanai, M. Yamanouchi, S. Ikeda, Y. Nakatani, F. Matsukura, and H. Ohno, Electric field-induced magnetization reversal in a perpendicular-anisotropy CoFeB-MgO magnetic tunnel junction, Appl. Phys. Lett. **101**, 122403 (2012).

[4] J. Zhu, J. A. Katine, G. E. Rowlands, Y. J. Chen, Z. Duan, J. G. Alzate, P. Upadhyaya, J. Langer, P. K. Amiri, K. L. Wang, and I. N. Krivorotov, Voltage-Induced Ferromagnetic Resonance in Magnetic Tunnel Junctions, Phys. Rev. Lett. **108**, 197203 (2012).

[5] Y. Suzuki, H. Kubota, A. Tulapurkar, and T. Nozaki, Spin control by application of electric current and voltage in FeCoMgO junctions, Phil. Trans. R. Soc. A **369**, 3658 (2011).

[6] D. Chiba, M. Sawicki, Y. Nishitani, Y. Nakatani, F. Matsukura, and H. Ohno, Magnetization vector manipulation by electric fields, Nature (London) **455**, 515 (2008).

[7] L. Gerhard, T. K. Yamada, T. Balashov, A. F. Takács, R. J. H. Wesselink, M. Däne, M. Fechner, S. Ostanin, A. Ernst, I. Mertig, and W. Wulfhekel, Magnetoelectric coupling at metal surfaces, Nat. Nanotechnol. **5**, 792 (2010).

[8] Y. Yamada, K. Ueno, T. Fukumura, H. T. Yuan, H. Shimotani, Y. Iwasa, L. Gu, S. Tsukimoto, Y. Ikuhara, and M. Kawasaki, Electrically induced ferromagnetism at room temperature in cobalt-doped titanium dioxide, Science **332**, 1065 (2011).

[9] A. Sekine and T. Chiba, Electric-field-induced spin resonance in antiferromagnetic insulators: Inverse process of the dynamical chiral magnetic effect, Phys. Rev. B **93**, 220403(R) (2016).

[10] E. Rashba, Properties of semiconductors with an extremum loop. 1. Cyclotron and combinational resonance in a magnetic field perpendicular to the plane of the loop, Sov. Phys. Solid State **2**, 1109 (1960).

[11] A. Manchon, H. C. Koo, J. Nitta, S. M. Frolov, and R. A. Duine, New perspectives for Rashba spin-orbit coupling, Nat. Mater. **14**, 871 (2015).

[12] I. E. Dzyaloshinskii, Thermodynamic theory of weak ferromagnetism in antiferromagnetic substances, Sov. Phys. JETP **5**, 1259 (1957).

[13] T. Moriya, Anisotropic Superexchange Interaction and Weak Ferromagnetism, Phys. Rev. **120**, 91 (1960).

[14] R. Skomski, A. Kashyap, and A. Enders, Is the magnetic anisotropy proportional to the orbital moment?, J. Appl. Phys. **109**, 07E143 (2011).

[15] J. Jensen and A. R. Mackintosh, *Rare Earth Magnetism* (Clarendon, Oxford, 1991).

[16] S. Blundell, *Magnetism in Condensed Matter* (Oxford University, New York, 2012).

[17] R. Skomski, *Simple Models of Magnetism* (Oxford University, New York, 2008).

[18] R. Skomski and J. M. D. Coey, *Permanent Magnetism* (Institute of Physics, Berkshire, 1999).

[19] R. Skomski and D. J. Sellmyer, Anisotropy of rare-earth magnets, J. Rare Earths **27**, 675 (2009).

[20] Y. Shiota, S. Murakami, F. Bonell, T. Nozaki, T. Shinjo, and Y. Suzuki, Quantitative evaluation of voltage-induced magnetic anisotropy change by magnetoresistance measurement, Appl. Phys. Express **4**, 043005 (2011).

[21] M. Tsujikawa, S. Haraguchi, and T. Oda, Effect of atomic monolayer insertions on electric-field-induced rotation of magnetic easy axis, J. Appl. Phys. **111**, 083910 (2012).

[22] See Supplemental Material at http://link.aps.org/supplemental/10.1103/PhysRevLett.120.027201 for different derivations of the voltage coupling energy and magnetization torque that support the simple interface potential step model. Supplemental Material includes Refs. [23,24]. We also give details of the numerical integration of the voltage-induced magnetization dynamics.

[23] S. Zhang, Spin-Dependent Surface Screening in Ferromagnets and Magnetic Tunnel Junctions, Phys. Rev. Lett. **83**, 640 (1999).

[24] W. H. Press, S. A. Teukolsky, W. T. Vetterling, and B. P. Flannery, *Numerical Recipes in C: The Art of Scientific Computing* (Cambridge University Press, Cambridge, England, 1992).

[25] A. A. Baker, A. I. Figueroa, G. van der Laan, and T. Hesjedal, Tailoring of magnetic properties of ultrathin epitaxial Fe films by Dy doping, AIP Adv. **5**, 077117 (2015).

[26] W. Zhang, D. Zhang, P. K. J. Wong, H. Yuan, S. Jiang, G. van der Laan, Y. Zhai, and Z. Lu, Selective tuning of Gilbert damping in spin-valve trilayer by insertion of rare earth nanolayers, ACS Appl. Mater. Interfaces **7**, 17070 (2015).

[27] C. Tang, P. Sellappan, Y. Liu, Y. Xu, J. E. Garay, and J. Shi, Anomalous Hall hysteresis in Tm3Fe5O12/Pt with strain-induced perpendicular magnetic anisotropy, Phys. Rev. B **94**, 140403(R) (2016).

[28] N. W. Ashcroft and N. D. Mermin, *Solid State Physics* (Brooks-Cole, Belmont, MA, 1976).

[29] R. Metselaar and P. K. Larsen, High-temperature electrical properties of yttrium iron garnet under varying oxygen pressures, Solid State Commun. **15**, 291 (1974).

[30] H. Pascard, Fast-neutron-induced transformation of the $Y_3Fe_5O_{12}$ ionic structure, Phys. Rev. B **30**, 2299(R) (1984).

[31] C. Song, B. Cui, F. Li, X. Zhou, and F. Pan, Recent progress in voltage control of magnetism: Materials, mechanisms, and performance, Prog. Mater. Sci. **87**, 33 (2017).